Refining of atmospheric transport model entries by the globally observed passive tracer distributions of [85]krypton and sulfur hexafluoride (SF$_6$)

Ingeborg Levin and Vago Hesshaimer

Institut für Umweltphysik, University of Heidelberg, Heidelberg, Germany

Abstract. Our high precision database of the global distribution of SF$_6$ in the troposphere [*Maiss et al.*, 1996] is used in a two-dimensional atmospheric transport model (2D-HD model) to study the behavior of this new tracer in comparison to the classical global atmospheric transport tracer krypton 85. The 2D-HD model grid has been derived from the three-dimensional Hamburg TM2 model with the same resolution in the vertical and meridional direction and was designed to run on any standard personal computer. The same vertical convection scheme and wind fields as in the TM2 model, reduced to two dimensions, were used in the calculations. In addition, the horizontal diffusion parameter of the model was adjusted by matching the model-estimated mean meridional [85]Kr distribution with observations over the Atlantic Ocean. To simulate global tropospheric SF$_6$ concentrations, an almost linearly increasing SF$_6$ source strength has been applied since 1970. The latitudinal distribution of the SF$_6$ source was assumed to be similar to the global electrical power production. Excellent agreement between SF$_6$ model results and observations is achieved with the [85]Kr-tuned 2D-HD transport model with respect to the global meridional concentration distribution, and particularly in middle to high northern latitudes. In the southern hemisphere at the German Antarctic station Neumayer, a significant seasonal cycle of SF$_6$ has been observed which is reproduced by the model, however, with a smaller amplitude. This finding may point to possible shortcomings of the model's transport scheme when simulating the seasonality of stratosphere-troposphere exchange in high southern latitudes.

Introduction

Atmospheric transport models are considered a powerful tool to investigate biogeochemical cycles of trace constituents such as carbon dioxide or methane. As they link hypotheses about sources and sinks to atmospheric observations, a crucial prerequisite of these models is their capability to correctly simulate atmospheric transport processes. The transport behavior of atmospheric models is therefore often tested through so-called atmospheric transport tracers and their global distributions. The radioactive isotopes [85]Kr and radon 222 ([222]Rn) as well as inert (long-lived) halocarbons are the classical tracers for this purpose [*Jacob et al.*, 1987; *Prather et al.*, 1987; *Heimann and Keeling*, 1989; *Zimmermann et al.*, 1989; *Feichter and Crutzen*, 1990; *Tans et al.*, 1990] as they have relatively well-defined source-sink characteristics, and their global atmospheric distributions have been thoroughly measured [e.g., *Weiss et al.*, 1992; *Cunnold et al.*, 1994].

Recently, a new tracer gas has been added to this potpourri, namely, the solely man-made and steadily increasing trace gas sulfur hexafluoride (SF$_6$) [*Maiss and Levin*, 1994]. Quasi-continuous atmospheric observations of SF$_6$ are now available for several years from globally distributed sites in the northern (Alert, 82°N; Fraserdale, 50°N; Izaña, 28°N) as well as in the southern hemispheres (Cape Grim, 41°S; Neumayer, 71°S) [*Maiss et al.*, 1996]. This observational SF$_6$ database was now used in combination with global observations of [85]Kr [*Weiss et*

al., 1992] in a simple exercise performed with our two-dimensional model of atmospheric transport (2D-HD (HD, Heidelberg) model) [*Hesshaimer et al.*, 1989; *Hesshaimer*, 1990]. Meridional and vertical profiles as well as long-term trends and seasonal cycles have been compared with observations.

Our purpose was threefold. (1) We wanted to investigate the behavior of the new tracer SF$_6$ in direct comparison to the classical global tracer [85]Kr. SF$_6$ has a totally different source distribution, namely, it is emitted in industrialized areas from a large number of almost continuously distributed sources, in contrast to [85]Kr which has only a small number of point sources, mainly located in the northern hemisphere. (2) Through the comparison with [85]Kr, namely, fine-tuning the transport parameters of our model with [85]Kr observations, we wanted to test the hypothesis that the global SF$_6$ source distribution is closely related to electrical power production. By this we could provide a realistic source characterization of SF$_6$, necessary for future use of this tracer in more sophisticated three-dimensional transport models. (3) We wanted to assess potential shortcomings in the investigation of global trace gas budgets using two-dimensional model results which, for problems related to atmospheric variations observed on hemispheric scales, are often distinct enough if compared to three-dimensional models. Among others, this assessment is relevant when using our 2D-HD model to simulate the global distribution and temporal change of atmospheric [14]CO$_2$ which has only a limited observational database [*Levin et al.*, 1992] but can provide important constraints on the global carbon budget [*Hesshaimer et al.*, 1994].

Table 1. Yearly Mean ^{85}Kr Emissions 1975–1988 for Individual NFRPs and Model-Estimated Global Emissions All in 10^3 Ci yr^{-1}

Plant	1975	1976	1977	1978	1979	1980	1981	1982	1983	1984	1985	1986	1987	1988
1. Hanford, United States (46.6°N, 114.7°W)	294	250	108	291	283	276	212	95	214	268	251	251[e]	251[e]	251[e]
2. Idaho, United States (43.4°N, 112.1°W)	24	33	111	101	0	92	59	9	3	0	0[e]	0[e]	0[e]	0[e]
3. Savannah, Georgia (33.3°N, 81.7°W)	520	711	448	530	480	580	840	515	698	698	700	700[e]	700[e]	700[e]
4. Sellafield, United Kingdom (54.6°N, 3.6°E)	1200	1200	800	700	940	840	1400	1190	1129	1003	643	1441	919	1076
5. Marcoule, France (44.4°N, 4.5°E)	100	92	117	308	280	535	310	310	620	600	600[e]	600[e]	600[e]	600[e]
6. La Hague, France (49.0°N, 0.9°W)	657	343	669	786	642	825	969	1220	1356	730	1900	784	946	730
7. Karlsruhe, Germany (49.0°N, 8.4°E)	43	86	115	34	51	32	70	16	76	32	92	83	83[e]	83[e]
8. Tokai-Mura, Japan (36.5°N, 140.6°E)	0	0	0	60	0	280	110	190	90	180	270	351	324	73
9. Kyshtym, Russia (55.7°N, 60.6°E)														
Zimmermann et al.[a]	1440	2100	3070	3140	3660	3080	2620	3200	3020	4720*	4930*	⋯	⋯	⋯
This work[d]	1439	2109	3062	3136	3651	3069	2626	3212	3056	4905	4787	4834	5416	4764
Total Source														
Zimmerman et al.[a]	4278	4815	5438	5950	6336	6540	6590	6745	7388	8051	9116	⋯	⋯	⋯
Jacob et al.[b]	⋯	⋯	⋯	6000	6130	6270	6400	6530	6660	⋯	⋯	⋯	⋯	⋯
Heimann and Keeling[c]	4397	4782	5261	5765	6211	6524	6661	6648	6628	⋯	⋯	⋯	⋯	⋯
This work[d]	4277	4824	5430	5946	6327	6529	6596	6757	7424	8416	9243	8837	8657	8929

NFRP, nuclear fuel reprocessing plant. Releases for 1975–1986 from plants 1–8 were taken from *Rath* [1988], except for Tokai-Mura, where 1985 and 1986 emissions were taken from *UNSCEAR* [1993]. The 1985 and 1986 emissions for Sellafield and La Hague reported by *Rath* [1988] which were taken from *von Hippel et al.* [1986] compare within ±1% with those given in *UNSCEAR* [1993]. 1987 and 1988 emissions from Sellafield, La Hague, and Tokai-Mura were also taken from *UNSCEAR* [1993].

[a] Model-calculated values taken from *Zimmermann et al.* [1989, Figure 1a]; asterisk, value calculated with zero release from Tokai-Mura.
[b] *Jacob et al.* [1987].
[c] *Heimann and Keeling* [1989].
[d] This work: emission values were compiled for a 5.06×10^{18} kg of air atmosphere [*Prather et al.*, 1987]; the model run was started at January 1, 1975, with a uniform ^{85}Kr concentration of 0.525 Bq m^{-3}.
[e] Value set equal to the previous value.

Emission Database and Atmospheric Observations

Krypton 85

The radioactive noble gas ^{85}Kr today is mainly released to the atmosphere through nuclear fuel reprocessing plants (NFRPs). Its only relevant sink is radioactive decay with a mean radioactive life time of 15.6 years. All known NFRPs are located in the northern hemisphere between 33°N and 56°N; their locations are given in Table 1. Nevertheless, observational evidence at the two midlatitude southern hemispheric stations Cape Point (34°S) and Cape Grim (41°S) [*Weiss et al.,* 1992] clearly demonstrates that there must be one or several yet unidentified ^{85}Kr sources located in the southern hemisphere. Yearly mean ^{85}Kr emission rates from the eight major NFRPs in the western world until 1986, as summarized in Table 1, have been compiled by *Rath* [1988]. More updated numbers for La Hague, Sellafield, and Tokai-Mura are reported in *UNSCEAR* [1993]. For overlapping periods they compare within ±1% with the numbers compiled by *Rath* [1988]. Direct emission rates from Kyshtym (Russia) are not available yet. The values of *Zimmermann et al.* [1989] and our estimates listed in Table 1 (plant 9) have been calculated as the difference between the respectively determined total emissions and the known releases from the western plants 1–8. *Zimmer-*

mann et al. [1989] calculated the total emissions from their model, and we derived them likewise (as listed in Table 1) from the observed temporal change of the global atmospheric ^{85}Kr inventory. For comparison, Table 1 also shows the total ^{85}Kr releases calculated by *Jacob et al.* [1987] and by *Heimann and Keeling* [1989]. The spatial distribution of the ^{85}Kr sources for our model estimates was set according to the latitudes and strengths of plants 1–9 (Table 1).

Continuous observations of ^{85}Kr at several worldwide distributed stations are performed by the Institut für Atmosphärische Radioaktivität, Freiburg, Germany, and the data till the end of 1988 have been published by *Weiss et al.* [1992]. In the northern hemisphere we used the weekly integrated long-term observations at Miami (25°N, 10 m asl (above sea level), 1981–1988) and at Schauinsland (48°N, 1200 m asl, 1980–1988) for comparison with model simulations. In the southern hemisphere, only weekly grab samples from Neumayer Station (Antarctica, 71°S, 42 m asl, 1982–1987) were compared with model simulations, to determine the long-term trend and to investigate the seasonal cycle.

Nine observed meridional ^{85}Kr profiles sampled during ship cruises over the Atlantic Ocean at about 30°W between 1980 and 1987 [*Weiss et al.,* 1992] were used in addition to the quasi-continuous long-term station data. To allow direct inter-

comparison, observed and model-calculated profiles were normalized to October 1, 1983, by the following procedure: We calculated the long-term trend through the Neumayer observations (see Figure 4a) and added the difference in the long-term fit values for Neumayer between October 1, 1983, and the respective observation date to each observational ship cruise value. This method partly compensates the statistical uncertainty of individual profiles reflecting variations in meteorology not resolved in our 2D-HD model. Moreover, it takes into account the overall increase of interhemispheric concentration gradients, caused by a 50% overall increase of the source strength between 1980 and 1987.

Observed vertical ^{85}Kr profiles are only available for the small latitudinal zone between 43°N and 45°N (1°W–3°E), namely, southern France. A mean observed vertical profile, normalized to January 1, 1986, was calculated from the data in Table A-III of *Weiss et al.* [1992] for comparison with our model results at the respective latitude (compare Figure 2).

Sulfur Hexafluoride (SF$_6$)

Sulfur hexafluoride (SF$_6$) is a very long-lived (atmospheric lifetime $\tau > 800$ years [*Morris et al.*, 1995]), purely anthropogenic atmospheric trace gas. Its mean concentration in the atmosphere has increased by about 2 orders of magnitude in the last two decades, exceeding 3 ppt at the end of 1994 [*Maiss and Levin*, 1994; *Maiss et al.*, 1996]. About 80% of the global SF$_6$ release are presumably due to leakages, etc., in electrical insulations and switching, and the remaining 20% mainly come from degassing and purifying molten reactive metals [*Stordal et al.*, 1993]. The estimated mean banking time between production and release today is approximately 10 years [*Maiss and Levin*, 1994]. Because of these source characteristics the global distribution of SF$_6$ emissions is closely coupled with the global distribution of electrical power production. SF$_6$ emissions are thus quite continuously distributed over the world's industrialized areas, herein contrasting with the punctual ^{85}Kr emissions. The atmospheric lifetime of SF$_6$ with respect to chemical destruction in the mesosphere and dissolution losses in the world oceans is larger than 800 years [*Ko et al.*, 1993; *Ravishankara et al.*, 1993; *Morris et al.*, 1995]. This long lifetime is of great advantage for the application of SF$_6$ as atmospheric transport tracer if compared to halocarbons: the uncertainty upon atmospheric lifetimes of chlorofluorocarbons introduces additional errors when using them to validate atmospheric transport models [*Prather et al.*, 1987].

Quasi-continuous two-weekly integrated high-accuracy atmospheric SF$_6$ observations at three background stations in the northern hemisphere (Alert, 82°N, 187 m asl, 1993–1994; Fraserdale, 50°N, 200 m asl, 1994; Izaña, 28°N, 2367 m asl, 1991–1994) and spot measurements of SF$_6$ from two background stations in the southern hemisphere (Cape Grim, 41°S, 95 m asl, 1978–1994; Neumayer, 71°S, 42 m asl, 1986–1994), as well as from two meridional profiles of SF$_6$ over the Atlantic Ocean from 40°N to 71°S have recently been reported by *Maiss and Levin* [1994] and *Maiss et al.* [1996]. These data form the observational basis for our comparison with SF$_6$ model results.

Maiss and Levin [1994] reported global mean SF$_6$ emission rates increasing linearly with time from 1970 onward with an estimated value of 5×10^6 kg SF$_6$ per year around 1990. This estimate is based on the long-term quadratic concentration increase observed at Neumayer Station. For the SF$_6$ model run presented here, we calculated the time development of the global mean emission rate for 1970 to 1993 in a similar way as

Table 2. Yearly SF$_6$ Emission Rates (Q_{SF6} [10^6 kg SF$_6$ yr^{-1}]) As Used in the 2D-HD Model

Year	Q_{SF6}	Year	Q_{SF6}
1970	0.730	1982	3.302
1971	0.940	1983	3.518
1972	1.152	1984	3.735
1973	1.364	1985	3.951
1974	1.578	1986	4.168
1975	1.792	1987	4.38
1976	2.007	1988	4.602
1977	2.222	1989	4.818
1978	2.437	1990	5.035
1979	2.653	1991	5.252
1980	2.869	1992	5.469
1981	3.085	1993	5.686

Emission values were compiled for a 5.06×10^{18} kg of air atmosphere [*Prather et al.*, 1987]; the model run was started at January 1, 1970, with a uniform SF$_6$ mixing ratio of 0.036 ppt.

for ^{85}Kr: SF$_6$ emission rates were derived from the change of the global atmospheric SF$_6$ inventory by using the quadratic concentration increase trends at Neumayer, Cape Grim, and Izaña. We accounted for the stratosphere, containing 15% of the atmospheric air mass, with a mean lag time of 2.5 years, but assumed no loss of SF$_6$ due to chemical destruction or other processes. A linear increase with time of the global mean SF$_6$ emission starting in 1967 according to Q_{SF6} [10^6 kg yr^{-1}] $= 4.913 + 0.2133 * t$, t $=$ years after 1990.0 fits the observed quadratic increase in the atmosphere reasonably well. To account for small interannual concentration variations, source strengths slightly different from this linear curve have been used in our model estimates. These yearly release rates are listed in Table 2. A total atmospheric mass of 5.06×10^{18} kg air was used for this source strength estimate. The meridional distribution of the nearly linearly rising SF$_6$ source was assumed to be equivalent to the meridional distribution of electrical power production used by *Prather et al.* [1987] to determine the emission pattern of halocarbons (Table 3). No temporal change of this distribution was assumed during the modeled period, although one may expect slight changes of the relative contributions (NH, 95%; SH, 5%) from the respective hemispheres from the 1970s throughout the 1990s.

Model

The two-dimensional Heidelberg model of atmospheric transport (2D-HD model) has been developed to allow first-order comparisons between its results and observations [*Hesshaimer*, 1990]. It also provides preconstraining estimates for the results to be obtained by more sophisticated three-dimensional models. The model has been developed in cooperation with the Max-Planck Institut (MPI) für Meteorologie in Hamburg (M. Heimann, personal communication). It was designed to work on any IBM PC compatible computer.

Algorithm Scheme

All physical parameters of the Earth atmosphere are represented in the model as zonally averaged means, thus reducing the modeling space to two dimensions. Subdividing the atmosphere into boxes, the algorithm computes the air mass transport between these boxes on the basis of observed meteorological data. This scheme is appropriate to describe the mass flow transport of any tracer, as long as the main transport

Table 3. Meridional Distribution of SF$_6$ Emissions in Percent of the Global Mean

Box Number	Latitude Belt	Percent Emission
1	−90 to −86.1 (south)	0
2	−86.1 to −78.3	0
3	−78.3 to −70.4	0
4	−70.4 to −62.6	0
5	−62.6 to −54.8	0
6	−54.8 to −47.0	0
7	−47.0 to −39.1	0
8	−39.1 to −31.3	2.22
9	−31.3 to −23.5	2.22
10	−23.5 to −15.7	0.74
11	−15.7 to −7.8	0
12	−7.8 to 0	0
13	0 to 7.8	0
14	7.8 to 15.7	1.48
15	15.7 to 23.5	2.96
16	23.5 to 31.3	4.44
17	31.3 to 39.1	21.48
18	39.1 to 47.0	25.19
19	47.0 to 54.8	28.89
20	54.8 to 62.6	10.37
21	62.6 to 70.4	0
22	70.4 to 78.3	0
23	78.3 to 86.1	0
24	86.1 to 90 (north)	0

medium is the air. The model bases on a zonally integrated version of the continuity equation:

$$\int_\Sigma \cos\theta\, \partial_t(\rho c)\, d\sigma + \oint_{\partial\Sigma} \cos\theta\, \rho V c\, d\eta$$

$$- \oint_{\partial\Sigma} \cos\theta\, \rho K(\nabla c)\, d\eta + \text{CONVEC}$$

$$= \int_\Sigma \cos\theta\, Q_{vol}\, d\sigma + Q_{rest}/(2\pi R) \qquad (1)$$

where

Σ box surface;
$d\sigma$ surface element (scalar);
$\partial\Sigma$ border of box surface (scalar);
$d\eta$ border element (vector);
θ degree latitude;
ρ mean air density;
c mean mass of tracer per mass of air;
V mean wind velocity ($V = v, w$);
K_{ij} diffusion tensor;
Q_{vol} volume sources;
Q_{rest} additional sources;
R Earth radius;
CONVEC   vertical convection (see text).

The horizontal transport is derived from meridional wind fields (v) and horizontal diffusion (K_{yy}), whereas the vertical transport depends on vertical wind fields (w), vertical diffusion (K_{zz}), and vertical convection (CONVEC). Horizontal and vertical diffusion terms account for the temporal and spatial averaging when the real wind data are mapped into the model grid. The diffusion coefficients were set to be proportional to the standard deviations (σ_v, σ_w) of the input wind fields. The

off-diagonal elements of the diffusion tensor are set to zero according to *Zimmermann et al.* [1989]. The term labeled CONVEC represents vertical transport arising from dry and moist convective processes which are not resolved in the model's wind field. The explicit CONVEC scheme consists of a redistribution of mass between the boxes in a vertical air column during the model's time step [see *Prather et al.*, 1987].

Meteorological Data Fields

The model grid and the data fields bear strong resemblance to a three-dimensional atmospheric CO$_2$ transport model (TM2) in use at the MPI in Hamburg [*Heimann and Keeling*, 1989]. The model grid subdivides the atmosphere horizontally into 24 segments leading from south pole to north pole and vertically into nine layers covering the range between 984 and 10 hPa. The limits of the boxes are the same as the corresponding limits in the TM2. The wind field (v, w) and standard deviation data (σ_v, σ_w) used in our model are the zonally and monthly averaged TM2 fields (originally data from the Global Weather Experiment; see *Heimann and Keeling* [1989]) and are based on observations between December 1978 and November 1979. Besides the problem of data availability, it does not make too much difference to use real-time meteorological data for this study. The real-time wind fields when averaged longitudinally to two dimensions would be considerably smoothed out anyhow, and the 1978–1979 data set is quite representative for mean conditions.

Our CONVEC data (monthly averages) are the zonal means of the TM2 models (originally described by *Prather et al.* [1987]), corrected for the time step used in our model. The air density data (monthly averages) have been computed on the basis of temperature and pressure fields [*Houghton*, 1977]. The meridional wind data field (v) has been slightly modified to insure air mass conservation in each air column of the model. The vertical wind field (w) was then deduced from the horizontal wind data field to insure air mass conservation in each box of the model.

Free Parameter Setting

Tuning of the 2D-HD model was performed by determining optimal values for the only free parameters which we decided to take: the diffusion fields (K_{yy}, K_{zz}). These were determined by multiplying, respectively, the horizontal and vertical wind variances at each grid point i,j ($\sigma_v, \sigma_w)_{ij}$ (not CONVEC) with two constants a_v and a_w. In a first step we fixed a_v and a_w to obtain a plausible diffusion field [cf. *Hyson et al.*, 1980]. In a second step we made profit of the similitudes between the TM2 and our 2D-HD model: a parallel [85]Kr run of the two models was used to get improved values for the parameters a_v and a_w. The final fine-tuning of a_v and a_w was achieved by fitting optimally to observed meridional [85]Kr profiles.

Figure 1 shows the comparison of our [85]Kr model results with the cruise data (both data sets normalized to October 1, 1983; see data description above). The maritime [85]Kr observations over the Atlantic Ocean are not zonal means. However, because of the rather strong longitudinal mixing from west to east at the latitude of the major sources these data are still a very good approximation of the real zonal mean, at least south of the major [85]Kr source regions. On the other hand, adjusting the air mixing in our 2D-HD model to maritime observations makes it more reliable to correctly model other trace gases (e.g., CO$_2$ or CH$_4$) where observations are also biased toward maritime stations [e.g., *Conway et al.*, 1994].

The model results in Figure 1 were obtained by optimum adjustment (least squares fitting to observations) of only the horizontal diffusion parameter a_v. However, with this tuning we also obtained good agreement between the observed vertical distribution and our model results as shown in Figure 2. The corresponding parameters a_v and a_w from this "fine-tuned" model run were therefore adopted for all further ^{85}Kr and SF$_6$ runs which allow for a direct comparison of both transport tracers.

Refined inspection of the model results in comparison with the observations provides several important features to be discussed: north of about 40°N, the 2D-HD model ^{85}Kr results, although qualitatively reproducing the latitudinal pattern with a maximum at about 55°N, still shows systematically higher values than observed over the Atlantic Ocean. The reason for this discrepancy is that the model results represent real zonal mean concentrations which are, particularly north of 40°N, strongly influenced by the continental ^{85}Kr pileup close to the large point sources. To illustrate this fact, we included the observed mean ^{85}Kr level in central Europe represented by measurements at the most eastern station Cracow (Poland, 50°N, 20°E, 220 m asl) for mid-September to mid-October 1983 and its standard deviation in Figure 1. There is, indeed, a general substantial ^{85}Kr pileup of 0.05–0.1 Bq m^{-3} observed at this continental site if compared to Atlantic Ocean levels. We therefore come to the (trivial) conclusion that our 2D-HD model will neither simulate maritime nor continental ^{85}Kr concentration levels in midnorthern latitudes correctly, at least for the lowest tropospheric levels between 40° and 70°N (see, however, SF$_6$ results below). At 50°N the model results do, however, seem to represent the observed zonal mean accurately, if estimated as lying between the mean of Atlantic Ocean and Cracow observations.

Modelling the Meridional Distribution of SF$_6$

Once the 2D-HD model was optimized through observed ^{85}Kr profiles, we could simulate the meridional distribution of

Figure 2. Comparison of vertical ^{85}Kr profiles for 43°N. Squares, concentrations observed over France, averaged for each box level, and normalized to January 1, 1986. Circles, mean of model-calculated values for each individual observation normalized to January 1, 1986. Error bars correspond to the standard deviation of the individual observations/model results.

SF$_6$ using the emission scenario described above and listed in Tables 2 and 3. Figure 3a compares the observed meridional profile collected at the end of 1993 over the Atlantic Ocean [*Maiss et al.*, 1996] with the results calculated by the model for the lowest tropospheric box layer. Mean SF$_6$ concentrations for the end of 1993 (October to December) observed at Alert (82°N), Izaña (28°N), Cape Grim (41°S) and Neumayer (71°S) [*Maiss et al.*, 1996] are also included in Figure 3a. The height of all stations except Izaña lies within the lowest model layer. To inspect the model-predicted vertical decrease of concentration with height due to the ground location of the SF$_6$ sources, we also included the model estimate for 2367 m asl at the latitude of Izaña in Figure 3a. The predicted difference matches the difference between observations at Izaña Station and corresponding ship-based measurements, but this needs to be confirmed when more data will be available.

Figure 3b shows the meridional distribution of the yearly mean SF$_6$ concentrations in 1993 in comparison with model estimates. Here we also included a value for Fraserdale (50°N) which was extrapolated back from the observations during 1994. We used the mean difference of Fraserdale and Izaña in 1994 (0.14 ppt) and the trend from the Izaña curve to estimate that value. The general good agreement between SF$_6$ observations and our model results confirms that tuning horizontal diffusion with the observed SF$_6$ profile would provide a very similar value for the model's free parameter a_v. The data from Fraserdale, if they are representative for the mean SF$_6$ concentration at about 50°N, also nicely confirm the model predictions at the latitude where the strongest sources are located. Also the observations at Alert (82°N), at very high northern latitudes, are correctly reproduced by our 2D-HD model. This was not so obvious for ^{85}Kr north of about 60°N (see Figure 1) and may, in fact, be due to the more uniform release of SF$_6$ on the northern hemispheric continents and to missing significant sources north of about 65°N. This finding is very promising with respect to the validity of our 2D-HD model for CO$_2$ and
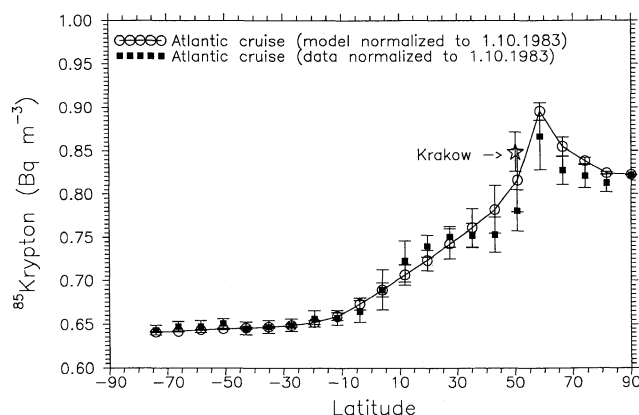

Figure 1. Comparison of meridional ^{85}Kr profiles at ground level. Squares, mean observed cruise data over the Atlantic Ocean for each of the meridional model box latitudes normalized to October 1, 1983 (see text). The star represents the mean value and standard deviation observed at Cracow Station, Poland (220 m asl), between mid-September and mid-October 1983. Open circles, mean concentrations as calculated by the 2D-HD model for the individual dates where cruise data exist, also normalized to October 1, 1983. Error bars correspond to the standard deviation of the individual observations/model results.
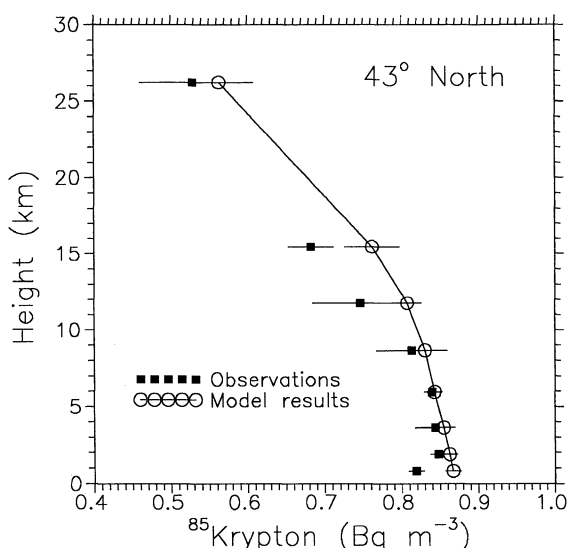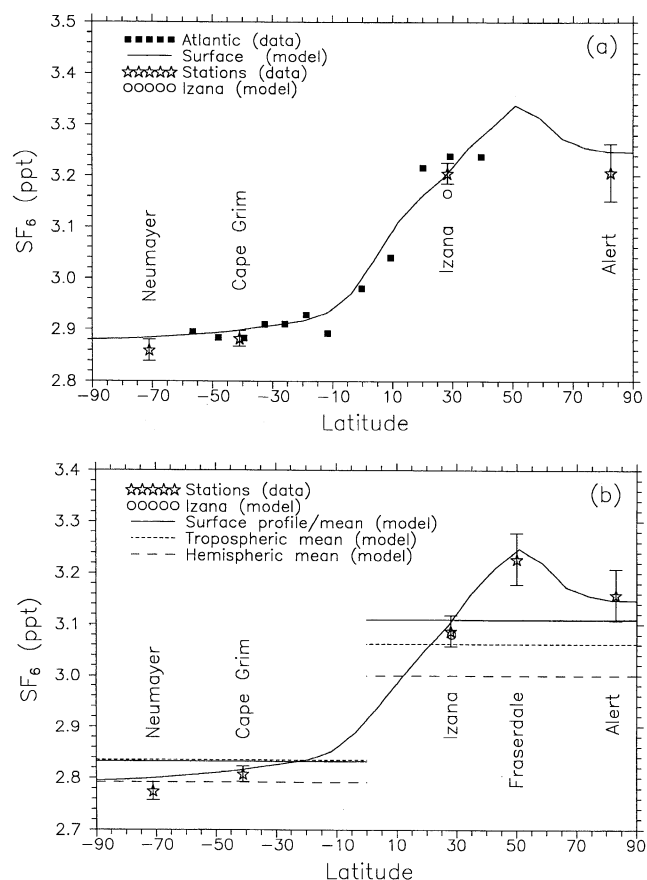
Figure 3. (a) Comparison of meridional SF$_6$ profiles for November 1993. Squares, observations over the Atlantic Ocean. Stars, mean station data for October to December 1993. Solid line, estimates for the model's surface layer. Circles, model estimate for Izaña Station (2367 m asl). (b) Comparison of 1993 yearly mean meridional profiles of SF$_6$. Stars, yearly means of station observations. The value for Fraserdale was extrapolated back from the observations during 1994, using the mean difference to Izaña in 1994 (0.14 ppt) as offset from the mean value for Izaña in 1993. Circle, model estimate for Izaña Station. Solid line, model calculations for the meridional profile, respectively, hemispheric means (horizontal lines) at the model's surface layer. Short-dashed horizontal lines, hemispheric means as calculated by the 2D-HD model for the respective troposphere; long-dashed horizontal lines, total hemispheric means. Error bars of the station data correspond to the mean standard deviations around individual trend curves (see Figure 5).

^{14}CO$_2$ model simulations for Alert and comparison with the respective observations [see *Levin et al.*, 1992] (but perhaps does not hold for CH$_4$ due to the high northern wetland sources still significant at latitudes north of 65°N). It is interesting to note from Figure 3b that the model-estimated mean ground level difference between the two hemispheres (solid horizontal line) nearly exactly represents the yearly mean SF$_6$ concentration difference observed between Izaña in the northern hemisphere and Cape Grim in the southern hemisphere.

Modeling Time Series of ^{85}Kr and SF$_6$ at Selected Monitoring Stations

Beside meridional and vertical profiles we also compared concentration records of ^{85}Kr and SF$_6$ at individual stations

with the 2D-HD model results. To compare the potentially different behavior of the two tracers ^{85}Kr and SF$_6$ with considerably different source distributions, it would be ideal to choose stations where long-term continuous measurements of both tracers have been published. Unfortunately, this is only the case for Neumayer Station in Antarctica. Among all published northern hemispheric long-term ^{85}Kr records, Miami (25°N, 10 m asl) shows the smallest influence from air masses with very high concentrations. These "spiked" air masses are not representative for their latitude as they were poorly dispersed longitudinally on the way from the respective NFRP point source. Krypton 85 observations at Miami can be compared with SF$_6$ model results at Izaña at approximately the same latitude but located in the free troposphere (28°N, 2367 m asl). At Miami, ^{85}Kr observations from 1981 to 1988 have been published [*Weiss et al.*, 1992], a time span which, however, does not overlap with the time span of published SF$_6$ data from Izaña (1991–1994) [*Maiss et al.*, 1996]. Even if the time spans for ^{85}Kr and SF$_6$ do only slightly or even not at all overlap, intercomparison of the general temporal behavior of both tracers is still feasible. This makes sense, as we, anyhow, do not use the actual meteorological data in individual years for the model estimates of trace gas concentrations.

Because of their vicinity to the sources, northern hemispheric stations need, however, a minimum of 4–5 years of continuous observations until we are able to pick up a mean seasonal behavior of SF$_6$ or ^{85}Kr with confidence. The Izaña, Fraserdale, and Alert SF$_6$ records are thus still too short, and their mean seasonal cycles show too much variance to be compared with the model estimates. To compare the seasonal cycles of model results with long-term observations at Miami and Neumayer for ^{85}Kr, and at Neumayer for SF$_6$, we calculated monthly mean values, deduced the long-term trends, and determined mean seasonal cycles by least squares curve fitting to a polynomial and harmonic function according to *Thoning et al.* [1989].

Long-Term Trends and Interannual Variations

Krypton 85. Figures 4a and 4b compare the interannual variations of ^{85}Kr observed at Neumayer, Miami, and Schauinsland with the corresponding 2D-HD model results. For comparison with the model results, the data from Miami have been selected to flag obvious outliers, respectively, samples that were influenced by direct emission plumes of nuclear fuel reprocessing plants. We rejected spikes more than 20 mBq higher than the original data filtered 60 times with a recursively applied binomial filter ($y'_i = 1/4 * (y_{i-1} + 2 * y_i + y_{i+1})$).

For Neumayer and Miami (Figure 4a) the observed absolute concentration level and the long-term increase are correctly reproduced by the model. For the most remote station, Neumayer at the Antarctic coast, this is, however, not surprising as the global ^{85}Kr emissions had been derived from the time development at Neumayer Station, and the meridional diffusion parameter had been adjusted in the model to reproduce shipboard measurements over the Atlantic Ocean, including observations at Neumayer. The good agreement between model and observations found for Miami, however, underpins both the representativeness of this station for the mean concentration at this latitude with respect to ^{85}Kr and the ability of the model to correctly predict the offset from Neumayer. As expected, however, our 2D-HD model is not able to reproduce the observed spikes resulting from direct transport of ^{85}Kr plumes from individual point sources to the observation site.

The effect of continental and regional [85]Kr sources is most obvious in the observations at the Schauinsland Station. Here the [85]Kr model estimates can only reproduce the lower envelope of observations (Figure 4b). The large seasonality seen in the data with pronounced maxima in summer and autumn which are caused by enhanced vertical mixing over the continent and therewith transport of ground level pollutants to the mountain site cannot be reproduced by the model. This feature of our 2D-HD model had already been identified when simulating the seasonal amplitude of CO_2 at the Schauinsland Station which was underestimated by more than 30% [*Hesshaimer et al.*, 1989].

SF$_6$. Figure 5 shows the comparison of the long-term increase of SF$_6$ observations at Neumayer, Cape Grim, Izaña, and Alert with model estimates. As already indicated in Figures 3a and 3b, the agreement between observed and modeled SF$_6$ concentrations is very good. Again, for the pure trend curve this is not surprising because we used the quadratic trend of Neumayer, Cape Grim, and Izaña data to estimate the time trend of the global SF$_6$ source strength. However, the perfect representation of the interhemispheric gradient confirms both that the meridional transport in the model is adequately parameterized and that the latitudinal partitioning of our SF$_6$ production scenario is reasonable. Also confirmed now on an
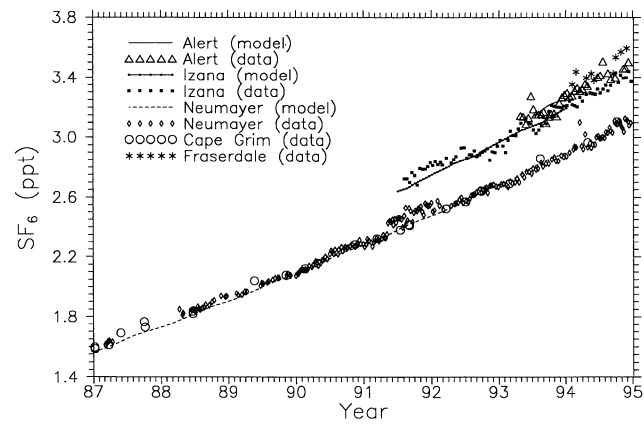

Figure 5. Comparison of observed (individual data points) and model-estimated (curves) long-term trends of SF$_6$ concentration for northern and southern hemispheric sites.

interannual timescale is the representativeness of Izaña for the mean concentration at that latitude, as we already pointed out above when discussing the SF$_6$ meridional profile for 1993.

Seasonal Cycles

In both estimates of global trace gas emissions ([85]Kr and SF$_6$) no seasonal variation had been taken into account. For SF$_6$ this assumption is justified because release of SF$_6$ in high-voltage electrical equipment is unlikely to show any seasonality. For [85]Kr emissions, seasonal variations have been reported for the La Hague reprocessing plant showing nearly zero releases in the summer months July and August [*Rath*, 1988; *Zimmermann et al.*, 1989]. As this source alone contributes about 15–20% to the global source (see Table 1), part of the observed seasonal variation at regional stations in western Europe may also be attributed to the seasonality of this source (see below).

Krypton 85. Although no seasonal variation in emissions has been assumed, a pronounced seasonal variation of [85]Kr at Miami is estimated by the model with lowest values during summer and highest concentrations in winter and spring. Figure 6a shows the deviations of observed respectively modeled monthly mean [85]Kr values from the respective long-term trends (modeled results and selected data of Figure 4a). As our model is restricted to two dimensions, only the seasonal changes in vertical and meridional transport are potentially reproduced. The striking agreement between model results and observations at Miami strongly suggests that the observed seasonal cycle of [85]Kr is caused by seasonal changes of the transport pattern: both the position of the Intertropical Convergence Zone (ITCZ) characterized by the steep concentration gradient between 30°N and 10°S (e.g., Figure 1) and/or the height of the boundary layer change with season. During winter, when the ITCZ is at its most southern location, Miami is largely influenced by the northern hemispheric regime (high [85]Kr concentrations), whereas during the summer, tropical air masses with lower [85]Kr activities are dominating at Miami. The seasonal amplitude we model for Miami underestimates the observations by about 30% which may be an indication that part of the variability is also caused by variations of the [85]Kr source. Within the year-to-year variability of the data, agreement between model and observations is, however, very satisfactory.
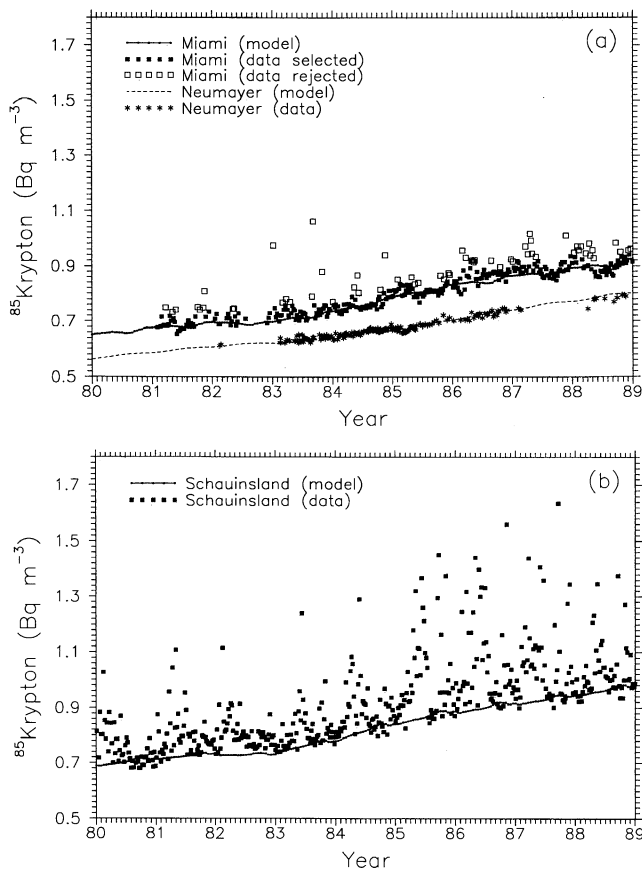

Figure 4. (a) Comparison of observed weekly integrated (individual data points) and model-estimated (curves) long-term trends of [85]Kr at Neumayer Station and Miami. For a more reliable comparison with model results, the Miami data have been selected for obvious outliers (plumes from nuclear fuel reprocessing plants; see text). (b) Same as Figure 4a except for the continental site Schauinsland.
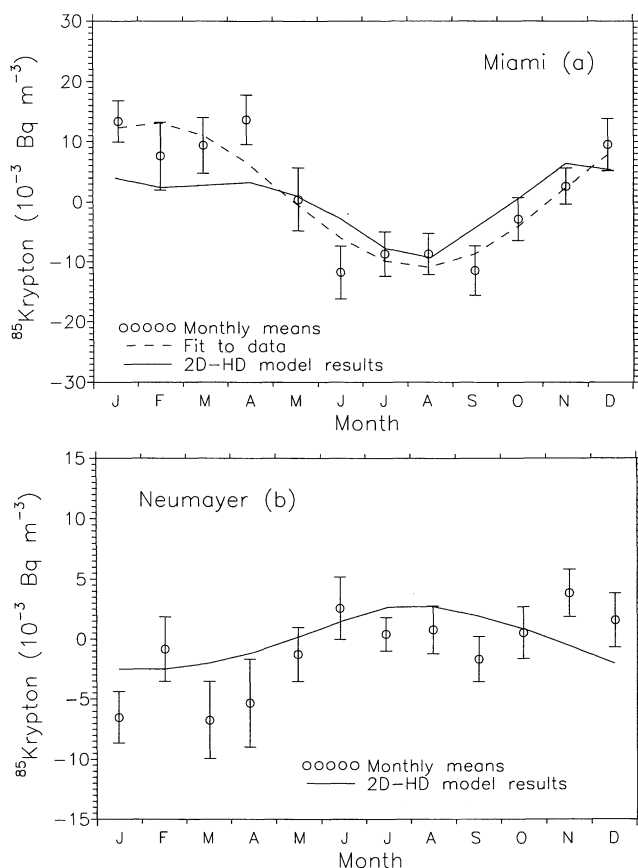
Figure 6. (a) 1981–1988 mean seasonal amplitude of selected monthly mean ^{85}Kr observations at Miami in comparison to the model estimate. (b) Same as Figure 6a but for unselected observations at Neumayer from 1983 to 1988. Error bars show the standard deviations of the mean, calculated from eight (Miami) respectively five (Neumayer) individual years.

Also at Neumayer Station in Antarctica, a small seasonal ^{85}Kr cycle is calculated by the model (Figure 6b). This predicted seasonality is also slightly indicated in the data; however, the November and December observations do not agree with the model estimates. The small seasonal amplitude postulated by the model for southern hemispheric stations may be attributed to variations in the interhemispheric transport being largest during the southern summer (December to February; compare Figure 8) when the ITCZ is moved northward therewith injecting high-concentration northern hemispheric air into the southern hemisphere. Also *Prather et al.* [1987] found a slight seasonality for CFC-11 concentration at Cape Grim which is in qualitative agreement with our model calculations.

SF$_6$. A significant seasonal variation is observed in SF$_6$ at Neumayer Station which is in phase but about 30% larger than predicted by the model (Figure 7). Besides the effect of a changing flux of northern hemispheric air to the southern hemisphere (see below and Figure 8), input of SF$_6$-depleted stratospheric air into the Antarctic troposphere is largest during late austral summer. This can be deduced from the seasonality of radioisotope ratios (^{10}Be/^{7}Be) showing a maximum at Neumayer Station at that time of the year (February) [*Wagenbach*, 1996]. The underestimated amplitude may be explained by a wrong parameterization of the seasonality of vertical exchange through both the Global Weather Experiment
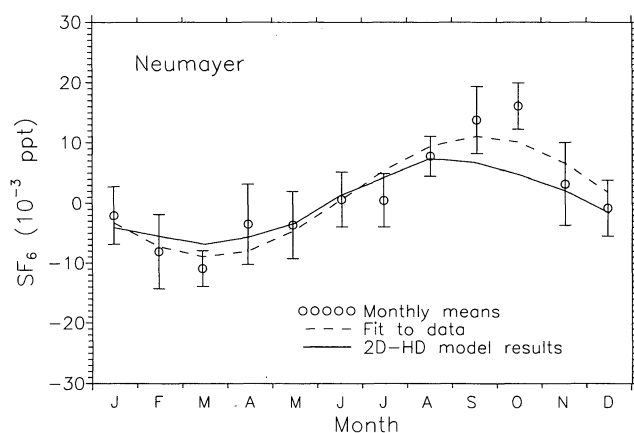

Figure 7. Mean seasonal amplitude of monthly mean SF$_6$ concentrations at Neumayer Station from 1988 to 1993 in comparison to model estimates. The period from February 1991 to February 1992 has been excluded in the analysis due to possible contamination of the samples [*Maiss et al.*, 1996]. Error bars show the standard deviations of the mean calculated from five individual years.

wind fields and the CONVEC transport scheme used in the Hamburg TM2 model and adopted for our 2D-HD model, particularly in high southern latitudes. The nicely resolved seasonal cycle of SF$_6$ observed at Neumayer Station now provides a powerful instrument to improve the transport parameters used in atmospheric models, particularly for these latitudes. This was not possible with the available ^{85}Kr data set [*Weiss et al.*, 1992] due to a significantly larger scatter in the observations at, e.g., Neumayer Station. The relative scatter of the ^{85}Kr data is about a factor of 2 larger if compared to the respective SF$_6$ scatter at that site. Part of the reason for the larger ^{85}Kr variability also at Neumayer, Antarctica, seems to be a yet unidentified ^{85}Kr source in the southern hemisphere leading to significant positive ^{85}Kr excursions at the Cape Point Station in South Africa [*Weiss et al.*, 1992]. Correct modeling of the transport is particularly crucial, e.g., to investigate the composite sources of CO$_2$ in middle to high latitudes of the
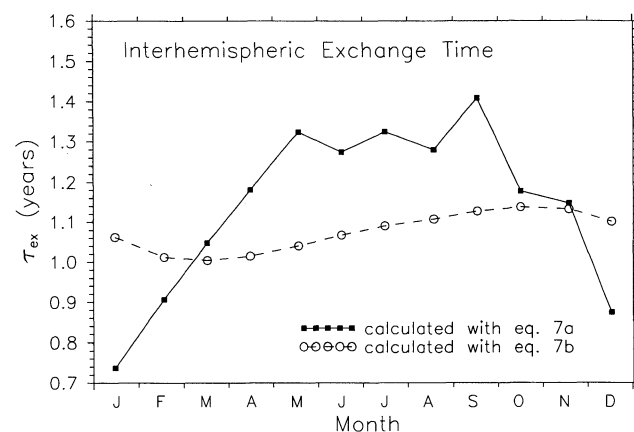

Figure 8. Seasonal cycle of the interhemispheric exchange time calculated for 1987 using ^{85}Kr as tracer. Results obtained with SF$_6$ as tracer are very similar. The solid line shows τ_{ex} calculated with equation (7a); the dashed line shows τ_{ex} calculated according to *Jacob et al.* [1987] when assuming $d/dt(c_{NH} - c_{SH}) = 0$ (equation (7b)).

southern hemisphere. Particularly concerning this aspect, SF_6 seems to be the most appropriate tracer to fulfill the task validating atmospheric transport models.

Interhemispheric Exchange

The interhemispheric exchange time τ_{ex} is an important parameter to characterize global atmospheric transport models. It was introduced to express the strength of the ITCZ acting as the major resistance of air mass exchange between the two hemispheres [e.g., *Bolin and Rodhe*, 1973]. Basically, it describes the inverse of the air mass fraction of one hemisphere transferred into the other hemisphere within the course of 1 year. Unfortunately, the value of τ_{ex} cannot be obtained from direct observations of air mass transport but has to be deduced indirectly from tracer observations. For tracers like ^{85}Kr or SF_6, mainly released to the atmosphere in the northern hemisphere and with atmospheric lifetimes τ_a much longer than τ_{ex}, the transport to the southern hemisphere is mainly controlled by the concentration offset between the two hemispheres. Therefore the hemispheric exchange time can be deduced from this offset provided the tracer release rate in both hemispheres is known.

Interhemispheric Exchange Time Deduced From Observations Using a Two-Box Model of the Atmosphere

Subdivision of the atmosphere into two well-mixed boxes, each representing one hemisphere, and with a gross air mass flow between the two boxes inversely proportional to τ_{ex} allows a first approach to estimate this parameter. This procedure, with little modeling effort, has been used in the past leading to values of τ_{ex} between 1 and 2 years from ^{85}Kr and SF_6 observations [e.g., *Weiss et al.*, 1983; *Jacob et al.*, 1987; *Maiss et al.*, 1996]. Comparing the results of their three-dimensional atmospheric transport model with ^{85}Kr observations over the Atlantic Ocean, *Jacob et al.* [1987] pointed out that the direct use of ground level ^{85}Kr observations to determine the interhemispheric concentration difference leads to τ_{ex} values systematically overestimated by about 50%. This is due to inappropriately neglecting the ^{85}Kr concentration decrease toward higher altitudes and in the stratosphere, particularly in the northern hemisphere.

For our two-box model approach, we use the simple tracer mass balance equations describing the variation of concentration in the two hemispheric boxes:

$$dc_{NH}/dt = 2 * Q_{NH}/\alpha - (c_{NH} - c_{SH})/\tau_{ex} - c_{NH}/\tau_a \quad (4a)$$

$$dc_{SH}/dt = 2 * Q_{SH}/\alpha + (c_{NH} - c_{SH})/\tau_{ex} - c_{SH}/\tau_a \quad (4b)$$

τ_a is the tracer's atmospheric lifetime; for ^{85}Kr, $\tau_a = 15.6$ years is the radioactive lifetime; for SF_6 we set $1/\tau_a = 0$ (no destruction); α is the conversion factor from tracer concentration c to the corresponding global atmospheric tracer mass inventory. If ^{85}Kr is expressed in Bq m^{-3} STP (1 Bq = 27 pCi) and Q in kCi (as in Table 1), $\alpha = 1.058 \times 10^5$. For SF_6 expressed in ppt (10^{-9} mol of SF_6 per moles of air) and Q in kg, $\alpha = 2.55 \times 10^4$. From (4a) and (4b) we have two choices to estimate τ_{ex} from mean hemispheric concentration time series:

$$\tau_{ex1} = (c_{NH} - c_{SH})/(2 * Q_{NH}/\alpha - dc_{NH}/dt - c_{NH}/\tau_a) \quad (5a)$$

$$\tau_{ex2} = (c_{NH} - c_{SH})/(dc_{SH}/dt + c_{SH}/\tau_a - 2 * Q_{SH}/\alpha) \quad (5b)$$

To estimate the mean hemispheric concentration time series, observations at individual sites are used. Differences in the interannual concentration changes (dc_i/dt) at different (background) sites within one hemisphere are small for both tracers, ^{85}Kr and SF_6, due to relatively fast mixing within hemispheres. The main uncertainty in the determination of τ_{ex} therefore is associated to the accuracy of the concentration difference between hemispheres ($c_{NH} - c_{SH}$).

We calculated mean hemispheric ^{85}Kr (surface) concentrations, from observed meridional profiles measured at ground level over the Atlantic Ocean (see Figure 1) using an appropriate areal weighting. All measured cruise data from *Weiss et al.* [1992] were normalized to October 1, 1983. From the observed meridional profiles we obtain a mean $\tau_{ex} = 1.6$ years with the two-box model approach. When applying the same areal weighting procedure to the 2D-HD model results corresponding to the cruise observations (also normalized to October 1, 1983; see Figure 1), we obtain a $\tau_{ex} = 1.7$ years with the two-box model approach. This value is slightly but not significantly higher than the τ_{ex} obtained directly from ^{85}Kr observations.

For the areal weighted meridional SF_6 profile observed at ground level over the Atlantic Ocean in November 1993 and extended northward by station data from Fraserdale (back extrapolated) and Alert (see Figure 3a and *Maiss et al.* [1996]), we obtain a value of $\tau_{ex} = 1.5$ years with the two-box model approach. The respective 2D-HD model results for the surface box layer, areal weighted and applied to the two-box model, lead to the same $\tau_{ex} = 1.5$ years. These results have still to be confirmed by more observations. However, the very good agreement between the interhemispheric exchange time derived from direct SF_6 surface measurements over the Atlantic Ocean, respectively, from 2D-HD model results for the surface box layer confirms that Atlantic SF_6 profiles are probably a good approximation for the real zonal means. This is less obvious for the tracer ^{85}Kr where the Atlantic observations seem to underestimate the real zonal mean at least north of 40°N (see Figure 1).

All results for the interhemispheric exchange time derived with the two-box model approach from mean hemispheric surface values of ^{85}Kr and SF_6 (observations and 2D-HD model results for the surface box layer) lie in the range of 1.5 to 1.7 years. Also for the 2D-HD model-estimated yearly mean surface ^{85}Kr profile in 1983–1984, we obtain a $\tau_{ex} = 1.5$ years. We therefore can confirm earlier estimates of the interhemispheric exchange time from *Weiss et al.* [1983], *Jacob et al.* [1987], and *Maiss et al.* [1996] when using surface data and a two-box model of the atmosphere.

Interhemispheric Exchange Time Deduced From the 2D-HD Model of the Atmosphere

In the 2D-HD model the net cross-equatorial tracer flux F_{eq} can be computed on a monthly basis. The interhemispheric exchange time can then be calculated from the northern hemispheric concentration offset relative to the southern hemisphere:

$$\tau_{ex} = \alpha/2 * (c_{NH} - c_{SH})/F_{eq} \quad (6)$$

Using (6) and ^{85}Kr, respectively, SF_6 as tracers, in both cases we obtain the same annual mean $\tau_{ex} = 1.1$ years. This interhemispheric exchange time is significantly smaller than the values we obtained from the two-box model approach and

mean surface data (τ_{ex} = 1.5 to 1.7 years) but agrees with the mean value reported by *Jacob et al.* [1987] (τ_{ex} = 1.1 years) obtained with their three-dimensional atmospheric transport model. As pointed out earlier by *Jacob et al.* [1987], the discrepancy between the two model approaches is mainly due to an overestimation of the real hemispheric means by surface observations. More rapid interhemispheric exchange in higher tropospheric and stratospheric levels of the atmosphere is only of minor importance. In fact, for anthropogenic trace gases with predominant sources in the northern hemisphere, it is the ground level concentration pileup in the northern hemisphere which is mainly responsible for overestimating ($c_{NH} - c_{SH}$). When using tropospheric means of SF$_6$ to calculate ($c_{NH} - c_{SH}$) and τ_{ex}, the interhemispheric exchange time is overestimated by only 10% if compared to values obtained with two- or three-dimensional models (compare Figure 3b where mean surface, tropospheric, and hemispheric values for SF$_6$ in 1993 are shown as horizontal lines).

Seasonal Variation of the Interhemispheric Exchange Time

The seasonal variation of net tracer transport over the ITCZ is one major reason for seasonal ^{85}Kr and SF$_6$ concentration variations observed at ground level at least in the southern hemisphere. F_{eq} determined by the transport field used in the 2D-HD model varies with season; the same is true for the northern hemispheric concentration offset with respect to the southern hemisphere ($c_{NH} - c_{SH}$). Both parameters lead to a seasonal variation of τ_{ex} in our 2D-HD model with an amplitude of ±30%. Weaker exchange is observed during the months April to September, whereas interhemispheric exchange is enhanced in the northern winter months (Figure 8). The seasonal amplitude of τ_{ex} seems to be stronger by a factor of 4 and phase shifted by 3 months if compared to the figures reported by *Jacob et al.* [1987] for their three-dimensional transport model. This obvious discrepancy seems to be caused by an artifact: *Jacob et al.* [1987] calculated the seasonal variation of τ_{ex} from the seasonal change of the global mean interhemispheric concentration difference using a linear relationship between τ_{ex} and ($c_{NH} - c_{SH}$) (dashed curve in Figure 8). This linear relationship is obtained from combining (4a) and (4b)

$$\tau_{ex} = ((Q_{NH} - Q_{SH})/(\alpha * (c_{NH} - c_{SH})) - d/dt(c_{NH}$$
$$- c_{SH})/(2 * (c_{NH} - c_{SH})) - 1/(2 * \tau_a))^{-1} \quad (7a)$$

and assuming $d/dt(c_{NH} - c_{SH})$ = 0. When also omitting the decay term $(1/(2 * \tau_a)$ = 0), we obtain the simplified equation (7b) which was used by *Jacob et al.* [1987, Figure 9]:

$$\tau_{ex} = \alpha * (c_{NH} - c_{SH})/(Q_{NH} - Q_{SH}) \quad (7b)$$

However, assuming $d/dt(c_{NH} - c_{SH})$ = 0 is not justified at all when studying the influence of the seasonal behavior of ($c_{NH} - c_{SH}$) on the seasonality of τ_{ex}. The appropriate equation to calculate the seasonal change of τ_{ex} is (7a). We therefore conclude that τ_{ex} indeed (also in the three-dimensional atmospheric model of *Jacob et al.* [1987]) is changing by a factor of 2 within the course of the year as illustrated in Figure 8. It is worth noticing that the seasonal cycle of SF$_6$ at Neumayer (Figure 7) cannot be explained simply from the variation of interhemispheric tracer transport. Considering the southern hemispheric troposphere as a well-mixed box we would deduce from τ_{ex} in Figure 8 a maximum tracer concen-

tration in the southern hemisphere during February to March, when the interhemispheric tracer transport (inversely proportional to τ_{ex}) passes its yearly mean value. Figure 7 shows that the seasonal cycle of SF$_6$ observed at Neumayer is just opposite to this prediction. It is well possible that the arrival of northern hemispheric air at the Antarctic coast in 71°S is delayed by several months. On the other hand, input of stratospheric air into the Antarctic troposphere is nearly immediately observed at ground level. As stated above, SF$_6$ at Neumayer shows concentration minima in late southern hemispheric summer, the time of the year when we observe maxima of stratospheric air at Neumayer station [*Wagenbach*, 1996].

Conclusions

The comparison of the 2D-HD model output with long-term observations of the two transport tracers ^{85}Kr and SF$_6$ has led to the following results:

1. The ^{85}Kr-tuned 2D-HD model led to excellent agreement with observations when estimating the meridional distribution of SF$_6$ at ground-based stations and over the Atlantic Ocean. Among others, this confirms our assumption that the SF$_6$ sources are distributed similarly to the global electrical power production.

2. The interhemispheric exchange time derived from mean ^{85}Kr and SF$_6$ observations at ground level when using a simple two-box model of the atmosphere (τ_{ex} = 1.5 to 1.7 years) is considerably larger by about 50% if compared to the exchange time derived from a latitudinally resolved transport model (in our 2D-HD model τ_{ex} = 1.1 years). This confirms the finding of *Jacob et al.* [1987] that hemispheric exchange times derived from two- and three-dimensional transport models cannot simply be applied to two-box models of the atmosphere if only surface observations are available. Using, however, tropospheric means leads to an overestimation of τ_{ex} of only 10% which is in the uncertainty range of estimates from high-resolution transport models.

3. The interhemispheric exchange time τ_{ex} shows strong seasonal variations with about 2 times higher values in the northern hemispheric summer (May to September) than in the northern hemispheric winter (December to February). Interhemispheric exchange times derived from single meridional profiles can therefore be strongly biased.

4. The new high-precision SF$_6$ database with extremely smooth time trends now opens new possibilities for transport model validation. This is obviously true for models simulating man-made trace emissions with similar distributions as SF$_6$ which could be seen from the perfect agreement between model estimates and observations particularly in the northern hemisphere. SF$_6$ therewith proofed to provide the most powerful and easy to measure transport tracer for future atmospheric applications.

References

Bolin, B., and H. Rodhe, A note on the concepts of age distribution and transit time in natural reservoirs, *Tellus*, *25*, 58–62, 1973.

Conway, T. J., P. P. Tans, L. S. Waterman, K. W. Thoning, D. R. Kitzis, K. A. Masarie, and N. Zhang, Evidence for interannual variability of the carbon cycle from the National Oceanic and Atmospheric Administration/Climate Monitoring and Diagnostics Laboratory global air sampling network, *J. Geophys. Res.*, *99*, 22,831–22,855, 1994.

Cunnold, D. M., P. J. Fraser, R. F. Weiss, R. G. Prinn, P. G. Simmonds, B. R. Miller, F. N. Alyea, and A. J. Crawford, Global trends and annual releases of CCl$_3$F and CCl$_2$F$_2$ estimated from ALE/GAGE and other measurements from July 1978 to June 1991, *J. Geophys. Res.*, *99*, 1107–1126, 1994.

Feichter, J., and P. J. Crutzen, Parameterization of vertical tracer transport due to deep cumulus convection in a global transport model and its evaluation with ^{222}Radon, *Tellus*, *42B*, 100–117, 1990.

Heimann, M., and C. D. Keeling, A three dimensional model of atmospheric CO$_2$ transport based on observed winds, 2, Model description and simulated tracer experiments, *Geophys. Monogr.*, *55*, 237–275, 1989.

Hesshaimer, V., A model to investigate the concentration of trace constituents in the earth atmosphere (in German), thesis, Inst. für Umweltphys., Univ. of Heidelberg, Germany, 1990.

Hesshaimer, V., I. Levin, and M. Heimann, Modeling the global distribution of CO$_2$ and ^{14}C in the atmosphere, in *Proceedings of the Third International Conference on Analysis and Evaluation of Atmospheric CO$_2$ Data Present and Past*, WMO Rep. 59, World Meteorol. Organ., Geneva, 1989.

Hesshaimer, V., M. Heimann, and I. Levin, Radiocarbon evidence for a smaller oceanic carbon dioxide sink than previously believed, *Nature*, *370*, 201–203, 1994.

Houghton, J. T., *Physics of the Atmosphere*, Cambridge Univ. Press, New York, 1977.

Hyson, P., P. J. Fraser, and G. I. Pearman, A two-dimensional transport simulation model for trace atmospheric constituents, *J. Geophys. Res.*, *85*, 4443–4456, 1980.

Jacob, D. A., M. J. Prather, S. C. Wofsy, and M. B. McElroy, Atmospheric distribution of ^{85}Kr simulated with a general circulation model, *J. Geophys. Res.*, *92*, 6614–6626, 1987.

Ko, M. K. W., N. D. Sze, W.-C. Wang, G. Shia, A. Goldman, F. J. Murcray, and C. P. Rinsland, Atmospheric sulfur hexafluoride: Sources, sinks, and greenhouse warming, *J. Geophys. Res.*, *98*, 10,499–10,507, 1993.

Levin, I., R. Bösinger, G. Bonani, R. J. Francey, B. Kromer, K. O. Münnich, M. Suter, N. B. A. Trivett, and W. Wölfli, Radiocarbon in atmospheric carbon dioxide and methane: Global distribution and trends, in *Radiocarbon After Four Decades: An Interdisciplinary Perspective*, edited by R. E. Taylor, A. Long and R. S. Kra, pp. 503–518, Springer-Verlag, New York, 1992.

Maiss, M., and I. Levin, Global increase of SF$_6$ observed in the atmosphere, *Geophys. Res. Lett.*, *21*, 569–572, 1994.

Maiss, M., L. P. Steele, R. J. Francey, P. J. Fraser, R. L. Langenfels, N.

B. A. Trivett, and I. Levin, Sulfur hexafluoride—A powerful new atmospheric tracer, *Atmosph. Environ.*, *30*, 1621–1629, 1996.

Morris, R. A., T. M. Miller, A. A. Viggiano, J. F. Paulson, S. Salomon, and G. Reid, Effects of electron and ion reactions on atmospheric lifetimes of fully fluorinated compounds, *J. Geophys. Res.*, *100*, 1287–1294, 1995.

Prather, M. J., M. B. McElroy, S. C. Wofsy, G. Russell, and D. Rind, Chemistry of the global troposphere: Fluorocarbons as tracers of air motion, *J. Geophys. Res.*, *91*, 6671–6681, 1987.

Rath, H. K., Simulation of the global ^{85}Kr and ^{14}CO$_2$ distribution by means of a time dependent two-dimensional model of the atmosphere (in German), Ph.D. thesis, Univ. of Heidelberg, Germany, 1988.

Ravishankara, A. R., S. Solomon, A. A. Turnipseed, and R. F. Warren, The atmospheric lifetimes of long-lived halogenated species, *Science*, *259*, 194–199, 1993.

Stordal, F., B. Innset, A. S. Grossmann, and G. Myhre, SF$_6$ as a greenhouse gas: An assessment of Norwegian and global sources and the global warming potential, *NILU-Rep. 15/93*, 27 pp., Norw. Inst. of Air Res., Lillestrom, Norway, 1993.

Tans, P. P., I. Y. Fung, and T. Takahashi, Observational constraints on the global atmospheric CO$_2$ budget, *Science*, *247*, 1431–1438, 1990.

Thoning, K. W., P. P. Tans, and W. D. Komhyr, Atmospheric carbon dioxide at Mauna Loa Observatory, 2, Analysis of the NOAA GMCC data, 1974–1985, *J. Geophys. Res.*, *94*, 8549–8565, 1989.

UNSCEAR, Report to the General Assembly, Sources and Effects of Ionizing Radiation, UNO, New York, 1993.

Von Hippel, F. D., H. Albright, and B. G. Levi, Quantities of fissile materials in U.S. and Soviet nuclear weapons arsenals, *Rep. PU/CEES 168*, Cent. for Energy and Environ. Stud., Princeton Univ., Princeton, N. J., 1986.

Wagenbach, D., Coastal Antarctica: Atmospheric chemical composition and transport, in *Processes of Chemical Exchange Between the Atmosphere and Polar Snow*, edited by E. Wolff and R. Bales, pp. 173–199, *NATO ASI Ser.*, vol. 43, Springer-Verlag, New York, 1996.

Weiss, W., A. Sittkus, H. Stockburger, H. Sartorius, and K. O. Münnich, Large-scale atmospheric mixing derived from meridional profiles of krypton 85, *J. Geophys. Res.*, *88*, 8574–8578, 1983.

Weiss, W., H. Sartorius, and H. Stockburger, Global distribution of atmospheric ^{85}Kr—A database for the verification of transport and mixing models, in *Isotopes of Noble Gases as Tracers in Environmental Studies*, pp. 29–62, Int. At. Energy Agency, Vienna, 1992.

Zimmermann, P. H., J. Feichter, H. K. Rath, P. J. Crutzen, and W. Weiss, A global three-dimensional source-receptor model investigation using ^{85}Kr, *Atmos. Environ.*, *23*, 25–35, 1989.

V. Hesshaimer and I. Levin (corresponding author), Institut für Umweltphysik, University of Heidelberg, Im Neuenheimer Feld 366, D-69120 Heidelberg, Germany.